



EVALUATION OF ITERATIVE ALGORITHMS FOR TOMOGRAPHY IMAGE RECONSTRUCTION

A. F. Velo^a; A. G. Alvarez^a; M. M. Hamada^a; C. H. Mesquita^a

^a *Instituto de Pesquisas Energéticas e Nucleares- IPEN/CNEN-SP. 05508-000, São Paulo, São Paulo, Brasil*

afvelo@usp.br

ABSTRACT

The greatest impact of the tomography technology currently occurs in medicine. The success is due to the fact that human body presents standardized dimensions with well-established composition. These conditions are not found in industrial objects. In industry, there is a great deal of interest in using the tomography in order to know the inner part of (i) manufactured industrial objects or (ii) the machines and their means of production. In these cases, the purpose of the tomography is: (a) to control the quality of the final product and (b) to optimize the production, contributing to the pilot phase of the projects and analyzing the quality of the means of production. This scan system is a non-destructive, efficient and fast method for providing sectional images of industrial objects and it is able to show the dynamic processes and the dispersion of the materials structures within these objects. In this context, it is important that the reconstructed image may present a great spatial resolution with a satisfactory temporal resolution. Thus, the algorithm to reconstruct the images has to meet these requirements. This work consists in the analysis of three different iterative algorithm methods, namely the Maximum Likelihood Estimation Method (MLEM), the Maximum Likelihood Transmitted Method (MLTR) and the Simultaneous Iterative Reconstruction Method (SIRT). The analyses involved the measurement of the contrast to noise ratio (CNR), the root mean square error (RMSE) and the Modulation Transfer Function (MTF), in order to know which algorithm fits the conditions to optimize the system better.

The algorithms and the image quality analyses were performed by Matlab® 2013b.

Keywords: Iterative Algorithms, Quality Evaluation, Industrial Tomography.

1. INTRODUCTION

Unlike the standard aspect of the computed tomography (CT) for medical application, industrial tomography systems applications should be adapted to the different size and geometry objects, usually placed in an aggressive environment, which contains flammable superheated or corrosive materials, and, eventually, subject to high internal pressure, all these factors bring in many difficulties for setting CT devices [1, 2]. In addition, the industrial systems involve multiphase dynamic processes containing solids, liquids and gases mixtures [3-7]. In other words, it is necessary to develop a tomographic system suitable for each industrial purpose [2, 6].

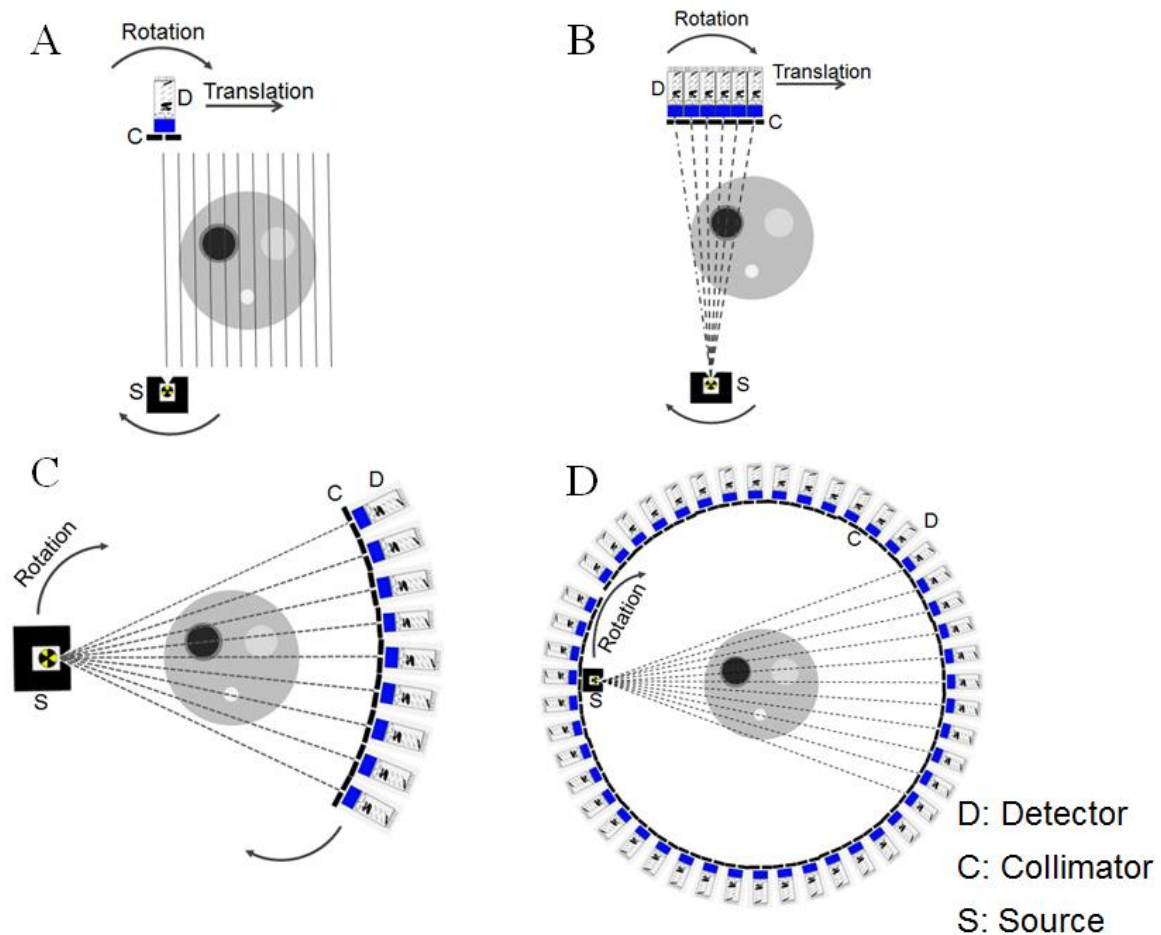
The CT systems based on transmission uses an array of encapsulated radioactive sources and detectors placed in opposite sides of the targeted object [7-9]. First generation tomography systems consist of a source emitting a collimated radiation pencil beam and a radiation detector (Fig.1a). The source-detector system moves in opposite sides of the object, measuring the attenuation of radiation at each position [10].

In the second generation CT systems, a set of detectors is placed opposite to the radioactive source with fan beam, moving (source and detector) around the object under study (Fig.1b) [10].

In the tomography of third generation, the source is collimated so that the path crossed by beams is similar to a fan (Fig.1c). The system rotates around the targeted object, obtaining a particular view for an "x" position of the source-detector array. In this type of system, several sources and arrays of multiple detectors may be used [10].

Finally, the so-called fourth-generation CT systems use a fixed array of detectors (a large number of detectors mounted on a fixed ring) and a radioactive source that rotates around the object (Fig.1d). Records of any measure are from the detector, representing a view of the object. However, all CTs are constituted, basically, of the same parts: radioactive sources; radiation detectors; a data acquisition system and a suitable computer [10].

Figure 1: (A) translation - rotation of a pencil beam (first generation), (B) translation - rotation of sources in a fan beam (second generation), (C) rotation of a fan-beam (third generation), (D) detector fixed - rotation source (fourth generation).

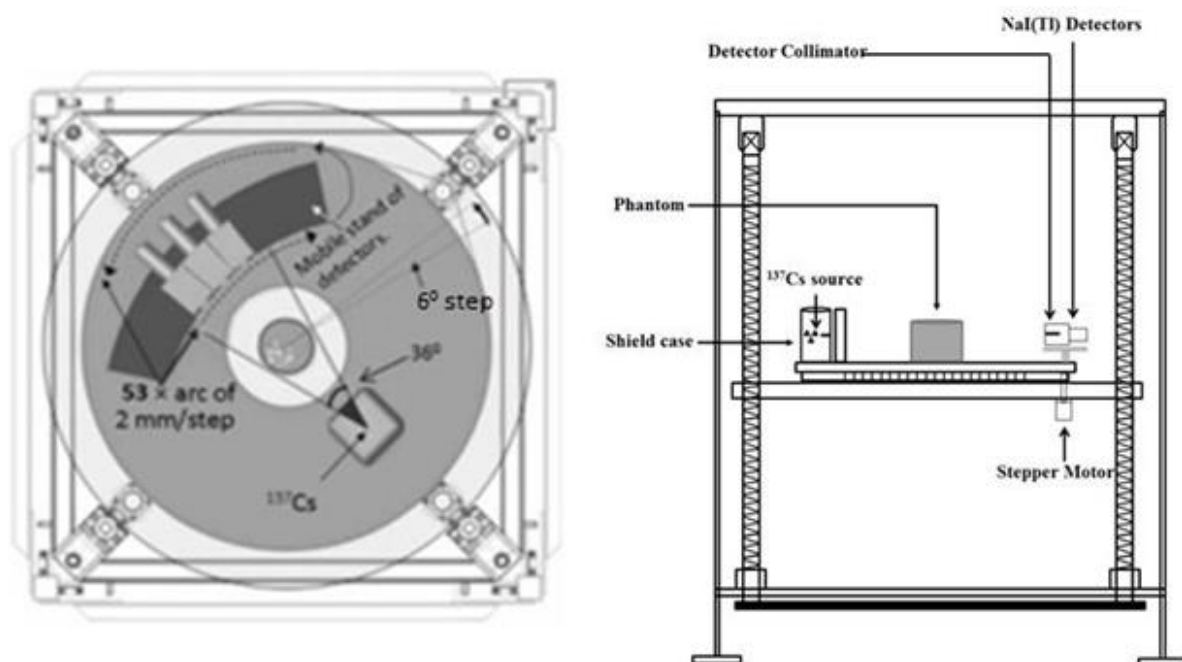


These scan systems are able to show the dynamic processes and the dispersion of the material structures within the objects. In this context, it is important that the tomography reconstructed image may present a great spatial resolution with a satisfactory temporal resolution [11, 12]. Thus, the algorithm selected to reconstruct the images has to meet these requirements. The aim of this work consists in the analysis of different iterative algorithms.

2. MATERIALS AND METHODS

A third generation computed tomography system, comprising three NaI(Tl) detectors of 50 x 50 mm² (diameter, thickness) shielded with lead, was used. The detectors were placed on a gantry in fan-beam geometry opposite to the gamma ray source, as shown in Fig.1. The three NaI(Tl) detectors were individually collimated with lead containing a septa of 2 x 5 x 50 mm³ (width, height, depth). The detectors move 53 times in a step angle of 0.226 degrees, emulating 159 detectors per projection. The counting time for sampling was 5 seconds. Thereafter, the support table containing the gantry and the ¹³⁷Cs gamma source (Fig. 1) rotates six degrees forward and this process goes on up to completing 360 degrees, totalizing 60 projections. For a total of 9540 samples (159 'virtual detectors' x 60 projections), the system spends 15,900 seconds or 4.4 hours to obtain each tomography image. The ¹³⁷Cs radioactive source, with an activity of 3.0 GBq (81 mCi), was placed into a radioactive shield-case with an aperture angle of 36 degrees (Fig. 2). This system had been previously described by Mesquita et al [12, 13].

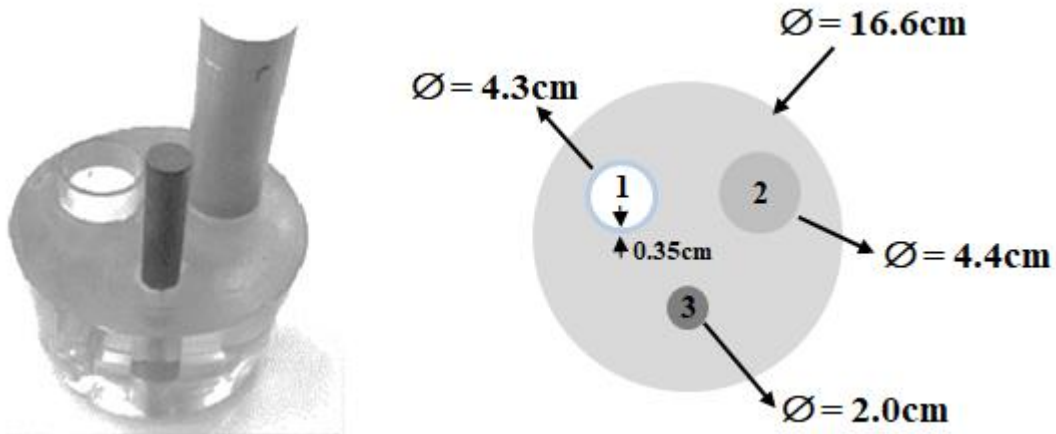
Figure 2: Diagram of the third generation CT scanner used. (a) top view and (b) side view [14]



A multiphase phantom was used to evaluate the performance of the multisource third generation tomography device [12]. The phantom consists of a polymethylmethacrylate (PMMA ($\rho \approx 1.19 \text{ g/cm}^3$)) solid cylinder

containing three holes: one filled with steel ($\rho \approx 7.874 \text{ g/cm}^3$), another with aluminum ($\rho \approx 2.698 \text{ g/cm}^3$) and a third one empty (filled with air) and surrounded with glass, as illustrated in Fig. 3.

Figure 3: Illustration of the multiphase phantom; (1) Air surrounded with glass wall; (2) aluminum bar; and (3) steel bar. The phantom is composed of PMMA.

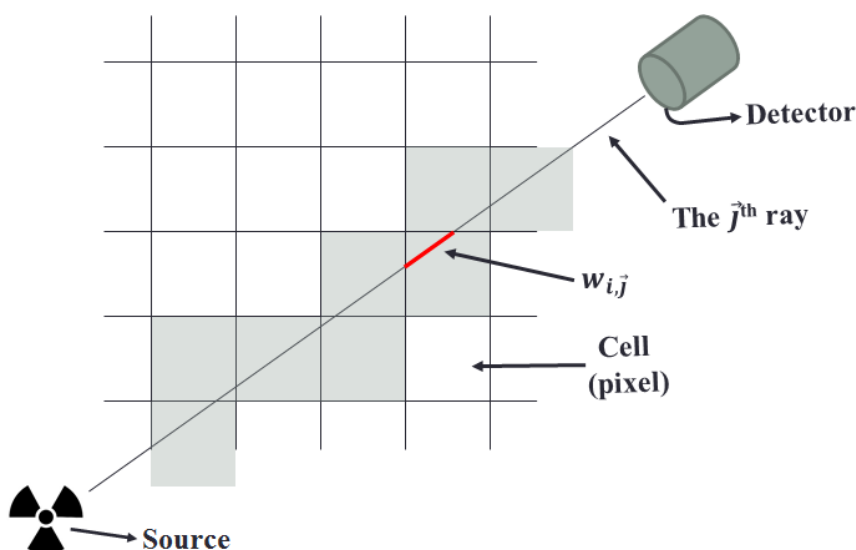


The image reconstruction is based on the exponential decay law defined by equation (1), which is known as Lambert-Beer's law [15]:

$$I = I_0 e^{-\sum_{i=1}^N \mu_i w_{i,j}} \quad (1)$$

where I_0 is the initial intensity of the beam radiation that focuses on the object at j direction, I is the intensity of the beam radiation through the object, N is the number of pixels on the matrix, μ_i is the linear attenuation coefficient of the matter and $w_{i,j}$ is the length of the beam radiation through pixel i and it is an element of the weighted matrix W [15]. Fig. 4 illustrates the scheme of the discretized grip to measure $w_{i,j}$.

Figure 4: Discretized grid



The discretized ray sum for each ray j ($j = 1, 2, \dots, J$) may be expressed as the equation (2) [15].

$$p_j^{normalized} = \ln\left(\frac{I_{oj}}{I_j}\right) = \sum_{i=1}^N w_{ij}\mu_i \quad (2)$$

The size of W is defined by the number of pixels in the reconstruction grid. Due to Poisson noise corruption of the measured data, a term η_j describing the noise is added to the equation (3) [15]:

$$p_j^{normalized} = \ln\left(\frac{I_{oj}}{I_j}\right) = \sum_{i=1}^N w_{ij}x_i + \eta_j \quad (3)$$

Solving a high number of linear equations, based on measurements corrupted by random variables and noise, requires the use of iterative algorithms. The iterative methods are divided in two categories, the algebraic and the statistical methods [15]. Algebraic reconstruction methods solve a set of linear equations by comparing the measured data set to an estimate and reducing the difference between them. Statistical methods reconstruct the image by implementing the maximization of the likelihood function, recognizing Poisson distribution function of the projections in relation with the measurements [15]. In the present work, the Simultaneous Iterative Reconstruction Technique (SIRT), the Maximum Likelihood Expectation Maximization (MLEM)

and the Maximum Likelihood Algorithm for Transmission Tomography (MLTR) were used to reconstruct the images, so that the first algorithm is an algebraic method and the last two are statistical methods.

The SIRT algebraic method is expressed by the equation (4) [15]

$$\mu_j^{(n+1)} = \mu_j^n + \delta \sum_{i=1}^M w_{ij} \frac{(g_i - \sum_{k=1}^N w_{ik} \mu_k^{(n)})}{\sum_{k=1}^N w_{jk}^2} \quad (4)$$

where, μ is the pixel index, δ is the relaxation parameter, g is the $P^{normalized}$ and w is the weighted matrix element.

The statistical methods, MLTR and MLEM, are expressed by equations (5) and (6), respectively [15].

$$\mu_j^{(n+1)} = \mu_j^{(n)} + \frac{\sum_{i=1}^M \left(w_{ij} \left(I_0 e^{(-\sum_{k=1}^N w_{ik} \mu_k^{(n)})} - I \right) \right)}{\sum_{i=1}^M \left(w_{ij} I_0 e^{(-\sum_{k=1}^N w_{ik} \mu_k^{(n)})} \sum_{k=1}^N w_{ik} \right)} \quad (5)$$

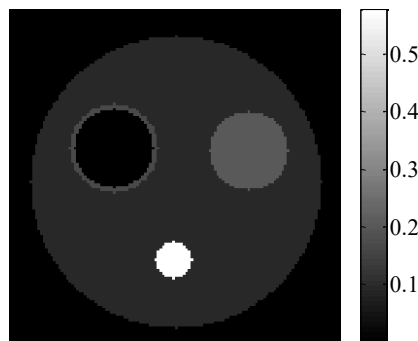
$$\mu_j^{(n+1)} = \frac{\sum_{i=1}^M \left[I_0 e^{(-\sum_{k=1}^N w_{ik} \mu_k^{(n)})} \left(1 - e^{-w_{ij} \mu_j^{(n)}} \right) \right]}{\sum_{i=1}^M \left[I_i - \bar{I}_i + 0.5(1 + e^{-w_{ij} \mu_j^{(n)}}) I_0 e^{(-\sum_{k=1}^N w_{ik} \mu_k^{(n)})} \right]} \quad (6)$$

All reconstruction was performed in a matrix of 128x128 pixels and 200 iterations. All physical measurements and reconstructions were performed by Matlab 2013b®. Root Mean Square Error (RMSE) was measured to evaluate which iterative algorithm approaches the pixel values, obtained experimentally for the theoretical values. This method is widely used to measure the quality of the image. The RMSE was obtained by equation (7) [16],

$$RMSE = \sqrt{\frac{\sum_{i=1}^N (\mu_i - \hat{\mu}_i)^2}{N}} \quad (7)$$

where, μ_i is the experimental pixel value obtained, $\hat{\mu}_i$ is the theoretical linear attenuation coefficient. The theoretical image is presented in Fig. 5.

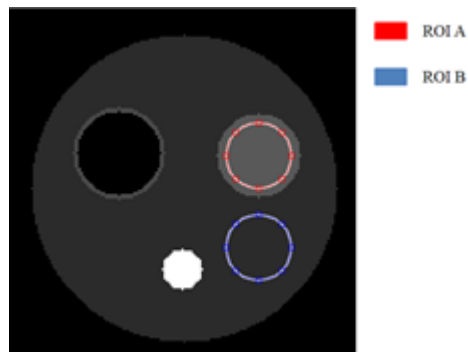
Figure 5: Theoretical image



The Contrast to Noise Ratio (CNR) was measured selecting regions of interest (ROIs) in the images of the phantom (Fig. 2) obtained, experimentally, for the different algorithms. A circular ROI was placed over the cylinder corresponding to the aluminum (ROI A) and another ROI, with the same size of ROI A, placed over the background, corresponding to the PMMA (ROI B), then the values of the CNR were obtained by equation (8) [16,17].

$$CNR = \frac{|\overline{\mu}_A - \overline{\mu}_B|}{\sqrt{\frac{\sigma_A^2 + \sigma_B^2}{2}}} \quad (8)$$

where, $\overline{\mu}_A$ is the mean pixel value of ROI A, $\overline{\mu}_B$ is the mean pixel value of ROI B, σ_A is the standard deviation of ROI A and σ_B is the standard deviation of ROI B. The ROIs are presented in Fig. 6, where the red circle represents ROI A and the blue circle represents ROI B.

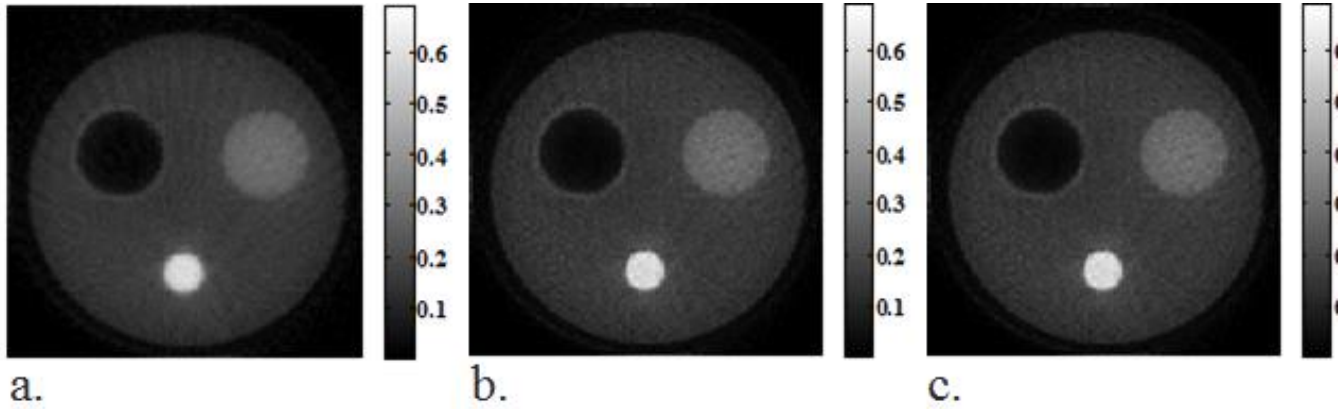
Figure 6: ROIs used to measure the CNR

The most comprehensive metric method used to measure and report spatial resolution of imaging systems is the modulation transfer function (MTF) [17-20]. Conventionally, the spatial resolution is estimated as the inverse of the value at 10% of MTF curve [17-20]. In the present work, the MTF was calculated using the Edge Spread Function, commonly known as ESF parameter [19, 20].

3. RESULTS AND DISCUSSION

The reconstructed images of the phantom obtained by the third generation industrial tomography are presented in Fig. 7, where Fig. 7a. represents the reconstruction by SIRT algorithm; Fig. 7b., by MLTR algorithm; and Fig. 7c., by MLEM algorithm.

Figure 7: Images reconstructed of the phatom using (a) SIRT algorithm; (b) MLTR algorithm and (c). MLEM algorithm



RMSE parameter, applied to perform the quality of the image for the three different algorithms (SIRT, MLTR and MLEM), was calculated using equation (7), comparing the experimental images with the theoretical image. Fig. 8 shows the curve behavior for each algorithm.

Figure 8: RMSE analysis for the three algorithms

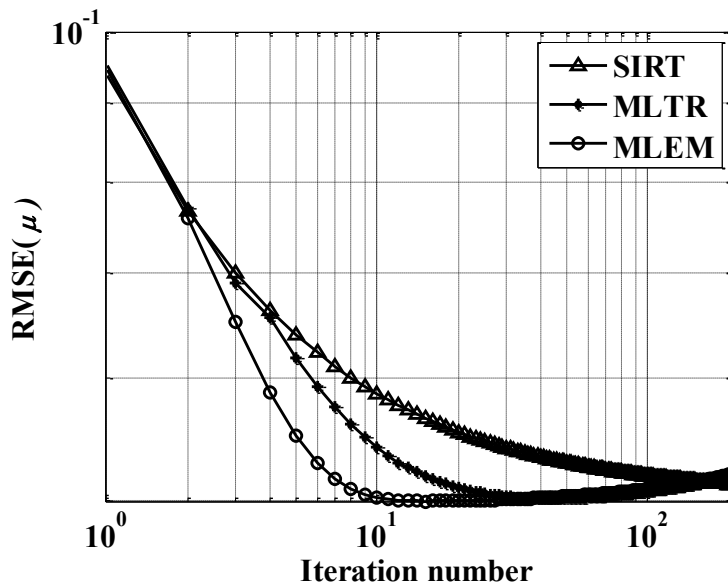
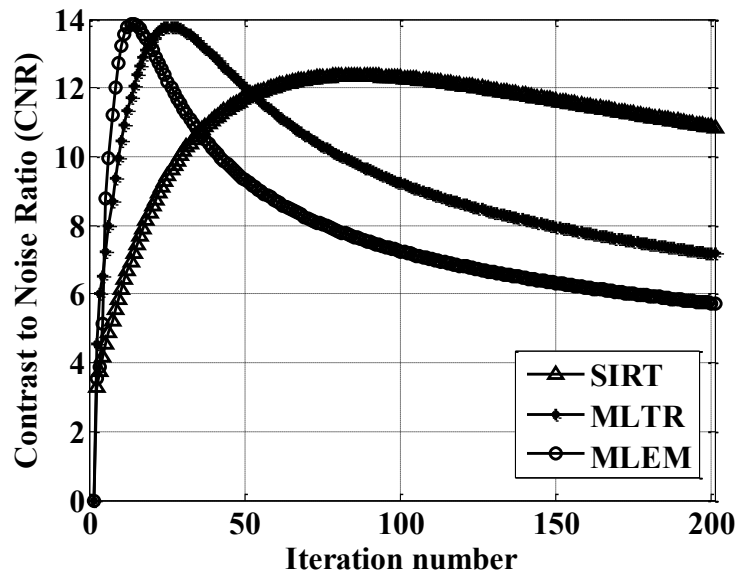


Fig 8 shows that the MLEM algorithm converges and approaches the theoretical values with fewer numbers of iteration compared to the other two algorithms. By this analysis, it is possible to observe that the images

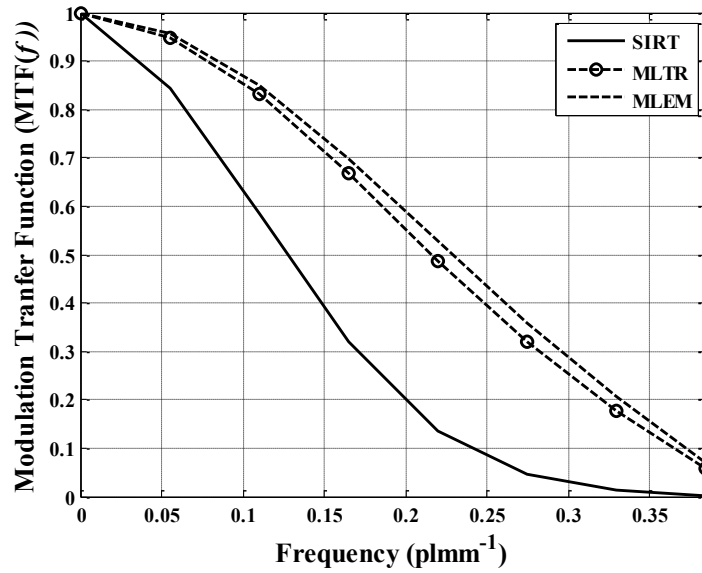
reconstructed by MLEM algorithm present better quality, converging their optimum with fewer numbers of iteration.

The analysis of the noise influence was performed by CNR parameter on the three different algorithms. The results are shown by Fig. 9. From this figure, it is possible to observe that even MLEM and MLTR algorithms reaching a higher CNR value in the first iterations, these values decrease as the number of iterations rises, different from SIRT algorithm, which reaches a lower CNR value, but decreases less than the others, what means that the noise influences less in the images reconstructed by the SIRT algorithm, as the number of iteration increases, when compared to the other two algorithms.

Figure 9: CNR analysis by the number of iterations



The spatial resolution of the reconstructed images was measured by the MTF (f). MTF curves, by the frequency spectrum (plmm^{-1}) of the three algorithms, at the iteration number of 200, are presented in Fig. 10.

Figure 10: MTF (f) of the three different algorithms, at the iterative number of 200

From Fig. 10, the MLEM algorithm presents a better spatial resolution in all the frequency spectra, compared to the other algorithms. The maximum spatial resolution of the system is measured at 10% of the MTF; in other words, the spatial resolution is calculated by the inverse of the frequency in 10% of the MTF. Thereby, the resolution for SIRT, MLTR and MLEM is about 2.86 mm, 2.75 mm and 2.70 mm, respectively.

Fig. 11 shows the area under the curve of the MTFs obtained for all iterative number of the three algorithms.

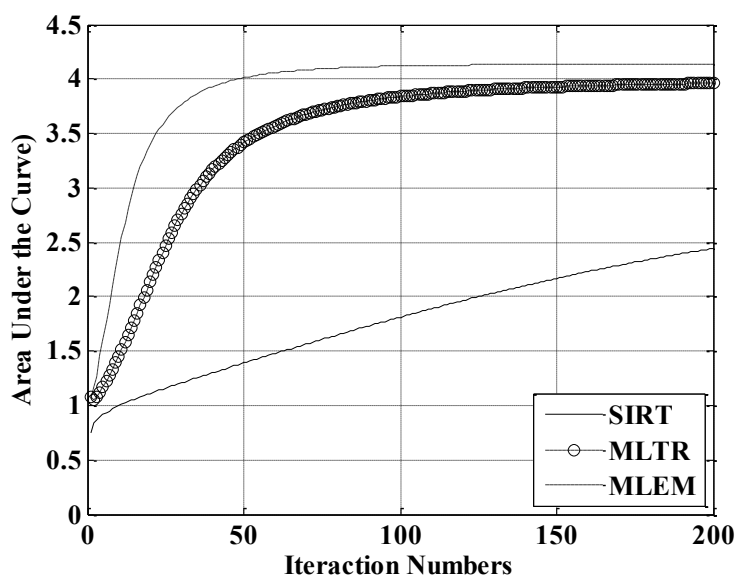
Figure 11: Area under the curve of the MTFs by the number of iterations

Fig. 11 shows that MLEM presents a better spatial resolution for all iterative numbers compared with the other algorithms. It is possible to observe, as well, that for the MLEM and the MLTR around 100 iterations, the spatial resolution reaches its optimum value and it maintains constant as the iteration numbers rises. This fact suggests that, for these two algorithms, the iterations could stop at 100, where the spatial resolution reached a higher value, reducing the time of reconstruction and avoiding the growth of noise, as observed in figure 9.

4. CONCLUSION

The results of RMSE values showed that the MLEM algorithm converges and approaches to the theoretical values with a lower number of iterations, compared to the other two algorithms, evidencing that this algorithm has a better image quality.

The CNR analysis showed that MLEM and MLTR algorithms reach a higher CNR value, but the number of iterations does not rise as the same, due to the growth of noise, different from the SIRT algorithm, that reaches a lower CNR value, but it decreases less than the others, what means that the noise has less influence on the images reconstructed by the SIRT algorithm than those by the other two algorithms.

The spatial resolution value obtained with SIRT, MLTR and MLEM algorithms is 2.86 mm, 2.75 mm and 2.70 mm, respectively, which means that the MLEM has a better spatial resolution.

The area under the curve of the MTFs for all number of iterations showed that at around 100 iterations, the spatial resolution for MLTR and MLEM reaches its optimum value, which means that for these two algorithms the iterations could stop at this value reducing time of reconstructing and avoiding the growth of noise. The SIRT algorithm has worse spatial resolution, and did not get its optimum value, suggesting that this algorithm has to keep iteration until reaches the optimum value.

For all the analysis measured, the MLEM showed to be a better algorithm to be applied on the systems of the third generation industrial tomography.

5. ACKNOWLEDGMENT

The authors express their acknowledgment to CNEN, FAPESP and the IAEA for the financial support. The authors, Carlos Henrique de Mesquita and Margarida Mizue Hamada, thank CNPq and Alexandre França Velo thanks CNEN, for their fellowship.

REFERENCES

1. CHAOUKI, J, LARACHI, F, DUDUKOVIC, M.P. Non-Invasive Monitoring of Multiphase Flows. In: CHAOUKI, J, LARACHI, F, DUDUKOVIC, M.P **Computer-assisted gamma and X-ray tomography: Application to multiphase flow In Non-Invasive Monitoring of Multiphase Flows**, 1st ed.; Elsevier: Amsterdam, The Netherlands, 1997; p 47 - 97.
2. MESQUITA, C. H.; VASQUEZ, P. A. S.; HAMADA, M. M. Multi-source third generation computed tomography for industrial multiphase flows applications. In: **IEEE Nuclear Science Symposium Conference Record**, 2011.
3. MESQUITA, C. H.; DANTAS, C.R., COSTA, F.E.; CARVALHO, D.V.S.; MADI, T. F; VASQUEZ, P. A. S.; HAMADA, M. M. Development of a Fourth Generation Industrial Tomography for Multiphase Systems Analysis. In: **IEEE Nuclear Science Symposium Conference Record**, p. 19-23, 2010.
4. KUMAR, S. B.; DUDUKOVIC, M. P. **Gas holdup in bubble columns at elevated pressure via computed tomography**. *Int. J. Multiphase Flows*, vol. 27, p.929-946, 2001.
5. ISMAILA; GAMIOG, J. C. **Tomography for multi-phase flow measurement in the oil indus-**

- try. Flow Measurement and Instrumentation, vol. 16, p. 145-155, 2005.
6. VASQUEZ, P.A.S.; MESQUITA, C. H.; HAMADA, M. M. **Methodological Analysis of Gamma Tomography System for Large Random Packed Columns**. Applied Radiation and Isotopes, v. 68, p. 658-661, 2010.
 7. IAEA-TECDOC-1589 **Industrial Process Gamma Tomography**, Viena, 2008
 8. CHAOUKI, J.; LARACHI, F.; DUDUKOVIC, M. **Noninvasive Tomographic and Velocimetry Monitoring of Multiphase Flows**. Industrial & Engineering Chemistry Research, v. 36, p. 4476-4503, 1997.
 9. JOHANSEN, G. A.; JACKSON, P. **Radioisotope Gauges for Industrial Process Measurements**. John Wiley & Sons, 2004.
 10. BUSHBERG, J.T., SEIBERT, J.A., LEIDHOLDT, E. M., BOONE, J.M. **The essential physics of medical imaging**. 3rd ed, Philadelphia, Lippicott Willians & Wilkins, 2001.
 11. CALVO, W. A. P.; HAMADA, M. M; SPRENGER, F. E.; VASQUEZ, P. A. S.; RELA, P. R.; MARTINS, J. F. T.; PEREIRA, J. C. S. M.; OMI, N. M.; MESQUITA, C. H., **Gamma-ray computed tomography scanners for applications in multiphase system columns**. Nukleonika; v. 54, p. 129-133, 2009.
 12. MESQUITA, C.H, VELO A.F., CARVALHO D.V.S., MARTINS, J.F.T., HAMADA, M.M. **Industrial tomography using three different gamma ray**. Flow measurement and instrumentation, v. 47, p. 1-9, 2016.
 13. MESQUITA, C.H., CARVALHO, D.V.S., KIRITA, R., SALAVDOR, P.A.V., HAMADA, M.M. **Gas-liquid distribution in a bubble column using industrial gamma-ray computed tomography**. Radiation Physics and Chemistry, v. 95, p. 396-400, 2014.
 14. VELO, A.F., CARVALHO, D.V.S., HAMADA, M.M. **Liquid Distribution and Holdup in the Random Packed Column**. Flow measurement and instrumentation. (in press).
 15. MAAD R., **Design Optimization of High Speed Gamma-Ray Tomography**. A dissertation submitted in partial fulfilment of the requirements for the degree of Doctor of Philosophy in Physics. Department of Physics and Technology University of Bergen Norway, 2009.
 16. VELO A.F, HAMADA M.M., CARVALHO D.V.S., MARTINS J.F.T, MESQUITA C.H. **A portable tomography system with seventy detectors and five gamma-ray sources in fan**

- beam geometry simulated by Monte Carlo method.** Flow measurement and instrumentation, v. 53, p. 89-94, 2017.
17. SMITH, STEVEN W. **The scientist and engineer's guide to digital signal processing.** 2nd ed, San Diego, California Technical Publishing, 1999.
 18. CHRISTIANSON O., CHEN, J. J.S., SAIPRASAD G., FILLIBEN, J.J, PESKIN A., TRIMBLE, C., SEIGEL, E L., SAMEI, E., **An improved index of image quality for task-based performance of CT iterative reconstruction across three commercial implementations.** Radiology. v. 275, p. 725-734, 2015.
 19. RICHARD S.L, HUSARIK D.B., YADAVA G., MURPHY S.N., SAMEI E. **Towards task-based assessment of CT performance: System and object MTF across different reconstruction algorithms.** Medical. Physics, v. 39, p. 4115 – 4122, 2012.
 20. SAMEI E., FLYNN M.J., REIMANN D.A. **A method for measuring the pre-sampled MTF of digital radiographic systems using an edge test device.** Medical Physics, v. 25, p. 102–113, 1998.